Proc. Natl. Acad. Sci. USA
Vol. 92, pp. 7051–7055, July 1995
Biochemistry

Binding studies of cationic thymidyl deoxyribonucleic guanidine to RNA homopolynucleotides

(antisense/antigene/hybrid duplex/triple helix)

KENNETH A. BROWNE, ROBERT O. DEMPCY, AND THOMAS C. BRUICE

Department of Chemistry, University of California, Santa Barbara, CA 93106

Contributed by Thomas C. Bruice, April 18, 1995

ABSTRACT **Deoxyribonucleic guanidine is a potential antisense agent that is generated via the replacement of the negative phosphodiester linkages of DNA [—O—(PO_2^-)—O—] with positively-charged guanidinium (g) linkages [—NH—C(=NH_2^+)—NH—]. A pentameric thymidyl deoxyribonucleic guanidine molecule [d(Tg)$_4$T-azido] has been shown to base pair specifically to poly(rA) with an unprecedented affinity. Both double and triple strands consisting of one and two equivalents of d(Tg)$_4$T-azido paired with one equivalent of poly(rA) are indicated by thermal denaturation experiments. At an ionic strength of 0.22, the five bases of d(Tg)$_4$T-azido are estimated to dissociate from a double helix with poly(rA) at >100°C! The effect of ionic strength on thermal denaturation is very pronounced, with stability greatest at low ionic strengths. The method of continuous variation indicates that there is an equilibrium complex with a molar ratio of d(Tg) to r(Ap) or d(Ap) of 2:1. Based on this evidence, models of the structures of d(Tg)$_9$T-azido bound to r(Ap)$_9$A are proposed.**

Putative drugs consisting of oligonucleotide analogs capable of arresting cellular processes at the translational or transcriptional level via base pair interactions with RNA or DNA are known as antisense and antigene agents, respectively (1–5). The backbones of viable antisense/antigene agents use linkages other than phosphodiesters due to the susceptibility of the backbones of RNA and DNA to degradation by cellular nucleases. To be effective, such agents must bind with fidelity to target nucleic acid sequences via Watson–Crick and Hoogsteen base pairing. Since antisense/antigene agents must compete with specific oligonucleotides and proteins for RNA/DNA targets, it is desirable that these agents have a high affinity for their complementary sequences. The stability of double- and triple-stranded RNA and DNA would increase if the electrostatic repulsion among the polyanionic single strands could be alleviated. This is seen in the enhanced binding of the noncharged peptide nucleic acids to single-stranded DNA (6, 7). One might suspect, therefore, that a strand of bases complementary to a nucleic acid sequence but connected together by positively charged linkages would act as a particularly effective antisense/antigene agent, since the repulsive effects found in duplexes of complementary nucleic acid strands would be replaced by attractive electrostatic interactions. Conversely, the electrostatic bonding between polycationic and polyanionic structures might be quite nonspecific and independent of complementary base pairing.

Recently we described the synthesis and binding properties of the pentameric thymidyl deoxyribonucleic guanidine (DNG) d(Tg)$_4$T-azido (**1**) (8–10), where g indicates a guanito linkage instead of a phosphate (p). Guanidinium groups [—NH—C(=NH_2^+)—NH—] replace the phosphodiester linkages [—O—(PO_2^-)—O—] of DNA to yield DNG. Both double and triple helical structures were formed between **1** and poly(dA). No helical structures were observed between **1** and poly(dG), poly(dC), poly(dT), or poly(dI). Most noteworthy was the unprecedented stability of the DNG·DNA complex. A double helix containing one equivalent of pentameric thymidyl DNG and one equivalent of poly(dA) does not dissociate in boiling water at near-physiological ionic strength. Our present studies focus on the potential of DNG as an antisense agent. The results of thermal denaturation and hybridization studies between DNG and RNA are provided as are modeling schemes representing anticipated structures of DNG·RNA complexes.

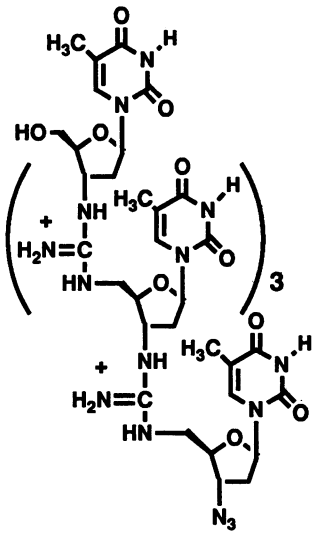

1

MATERIALS AND METHODS

Synthesis. Synthesis of d(Tg)$_4$T-azido (**1**) was as described (10).

Thermal Denaturation Studies. Plots of A_{260} vs. t (°C) for **1** in the presence of poly(rA), poly(rG), poly(rI), poly(rC), or poly(rU) were obtained at pH 7.0 (0.01 M $KHPO_4$ buffer) using a Perkin–Elmer UV/visible spectrophotometer in conjunction with a National Institute of Standards and Technology digital thermometer (accurate to ±0.2°C). The concentration of each of the oligonucleotides was 41.7 μM in bases. Concentrations of **1** and the polyoligonucleotides were determined spectrophotometrically from molar (nucleotidyl unit) extinction coefficients [8700 $M^{-1}\cdot cm^{-1}$ at 268 nm for **1** (11), 9800 $M^{-1}\cdot cm^{-1}$ at 258 nm for poly(rA), 10,400 $M^{-1}\cdot cm^{-1}$ at 253 nm for poly(rG), 10,200 $M^{-1}\cdot cm^{-1}$ at 248 nm for poly(rI), 6200 $M^{-1}\cdot cm^{-1}$ at 269 nm for poly(rC), and 9350 $M^{-1}\cdot cm^{-1}$ at 260 nm for poly(rU); values for the polyribonucleotides are

The publication costs of this article were defrayed in part by page charge payment. This article must therefore be hereby marked "*advertisement*" in accordance with 18 U.S.C. §1734 solely to indicate this fact.

Abbreviations: DNG, deoxyribonucleic guanidine; t_m, thermal denaturation temperature; ABNR, adopted basis Newton–Raphson.

courtesy of Pharmacia] and the Beer–Lambert law at 30°C and pH 7.5. The ionic strength (μ) of samples was adjusted using an appropriate concentration of KCl. In a typical experiment, a solution of **1** and a RNA polyoligonucleotide was heated to ≥93°C and allowed to cool to 5°C over several hours. Data points were then collected as the temperature was raised at the rate of ≈1°C/5 min. The data points that made up each curve were then computer fit to Eq. **1** (one hyperchromic transition) or Eq. **2** (two hyperchromic transitions),

$$A_{260} = \frac{a_1}{1 + e^{b_1(t - t_{m1})}} + d \quad [1]$$

$$A_{260} = \frac{a_1}{1 + e^{b_1(t - t_{m1})}} + \frac{a_2}{1 + e^{b_2(t - t_{m2})}} + d \quad [2]$$

which optimize for the inflection points of a curve (t_{m1} and t_{m2} in the case of DNG, where t_m is the thermal denaturation temperature), the change in absorbances between inflection points (a_1 and a_2), the slope coefficients (b_1 and b_2), and the absorbance at high temperature (d).

Stoichiometry of Binding. The stoichiometry of binding was determined by the method of continuous variation (12). Solutions containing the different molar ratios in d(Tg) (as **1**) and r(Ap) or d(Ap) [as poly(rA) or poly(dA), respectively] were heated to >90°C and allowed to slowly cool to 30°C over several hours. The total concentration in bases was always 50 μM. The pH was maintained at 7.0 with 0.01 M $KHPO_4$ buffer while the ionic strength was held constant at 0.12 with KCl. The absorbance of each solution at 260 nm was monitored on a Perkin–Elmer 553 UV/visible spectrophotometer at 30, 60, and 90°C (solutions were allowed to equilibrate at the next higher temperature for at least 15 min even though the absorbance reading stabilized in less than 5 min).

Molecular Modeling. All model building and computations were performed on a Silicon Graphics (Mountain View, CA) 4D/320GTX workstation using the molecular modeling program QUANTA, Version 4.0, and the molecular mechanics calculation program CHARMM, Version 21.3 (Molecular Simulations, Waltham, MA). The A-form of DNA generated in QUANTA was used for the initial coordinates in the construction of r(Ap)$_9$A·d(Tg)$_9$T-azido. A triple-helical model of d(pT)$_{10}$·d(pA)$_{10}$·d(gT)$_{10}$ (8) based on a theoretical structure of triple-helical DNA d(pT)$_{10}$·d(pA)$_{10}$·d(pT)$_{10}$ (13) served as a useful starting point for the modeling of d(Tg)$_9$T-azido·r(Ap)$_9$A·d(Tg)$_9$T-azido. The sugars of the purine strands were converted from deoxyriboses to riboses by replacing the H2′ protons with hydroxyl groups. Guanidinium groups [$(H_2N)C^+(NH)_2$] were overlapped on the phosphates (PO_4^-) of the nucleotide linkages of the pyrimidine strands. Two of the guanidinium nitrogen atoms overlap with O3′ and O5′ of the phosphate while the carbon atom is positioned near phosphorous. The $=NH_2$ is placed in between the two charged oxygens of $—PO_2^-—$. The phosphate moieties were deleted, and the guanidyl groups were attached to the 5′ and 3′ sugar carbons of successive deoxyribonucleotidyl units. Prior to minimizations, sodium ions (charge, +1.0) were placed adjacent to the phosphate moieties, and chloride ions (charge, −1.0) were placed near the guanidinium groups. Residue topology files (RTF) for the DNG thymidyl unit and termini were written by comparison with the DNAH.RTF file that accompanies the CHARMM program. Atom types of C, NC, and HC were used for the carbon, nitrogens, and hydrogens of the guanidinium moieties, respectively. The geometry of the 3′-azido termini on the DNG strands was held fixed based on the x-ray structure of tri-*O*-acetyl-β-D-xylopyranosyl azide [refcode ACXPAZ (14) from the Cambridge Structural Database (15)].

The modified backbone conformations were adjusted by applying 100 steps of steepest descents minimization followed by 500 steps of the adopted basis Newton–Raphson (ABNR) minimization algorithm with constraints on the atomic positions of the RNA strands and on the nucleobases of the DNG strands. Constraints were then sequentially removed (DNG nucleobases, then RNA strand) with distance constraints added between the base pairs while continuing to optimize the structure with the ABNR algorithm. Finally, the distance constraints were removed, and the ABNR algorithm was allowed to proceed until the root-mean-square derivative reached <0.5 kcal·mol^{-1}·Å^{-1}. Helical parameters were calculated with the NEWHEL93 program (16), which was generously provided by R. E. Dickerson (University of California, Los Angeles). This program was run with coordinates in Brookhaven's Protein Data Bank format based on the best helices generated from each of the sugar's C1′, the pyrimidine's N1, and the purine's N9 atoms. Calculation of the groove widths was based on the shortest distances between the phosphate and the guanidinium carbon atoms of annealed strands.

RESULTS AND DISCUSSION

Dissociation of DNG from RNA. In the thermal denaturation analysis of d(Tg)$_4$T-azido (**1**) bound to poly(rA), two distinct hyperchromic shifts were observed in the UV spectra of samples at high ionic strength (Fig. 1). Based on the precedence set in DNA and RNA thermal denaturation analysis (11), these transitions correspond to the denaturation of a triple-helical hybrid at 44.4, 50.2, and 53.2°C (μ = 0.62, 0.82, and 1.2, respectively) followed by denaturation of the duplex at 90.7, 90.4, and 82.4°C. At μ = 0.22 and 0.42, only one hyperchromic shift could be seen corresponding to a triple- to double-helical transition at 62.5 and 49.5°C, respectively. The second transition did not commence by 93°C at μ = 0.22 and, therefore, was estimated to be ≥100°C; at μ = 0.42, a second transition was not complete by 93°C and was tentatively assigned to be ≈100°C. At μ = 0.12, no transitions were seen as high as 93°C; the thermal stability is apparently so great that even the triple-helical structure of d(Tg)$_4$T-azido bound to poly(rA) (2:1) does not denature at near-boiling temperatures. This contrasts with the denaturation profiles of d(Tp)$_{15}$T bound to poly(rA); all have sharp, single denaturation transitions (36, 41, 47, and 49°C at μ = 0.12, 0.22, 0.62, and 1.2, respectively; plots not shown), which are slightly lower than the denaturation points with d(Tp)$_{15}$T bound to poly(dA) (9, 10). No hyperchromic shift was seen in the UV spectra of a solution between approximately 1 and 93°C, which contained d(Tg)$_4$T-azido and either poly(rG), poly(rC), poly(rU), or poly(rI) (examined at both μ = 0.12 and 1.2 at pH 7.0). There was a hyperchromic shift centered at ≈5°C that was due to the denaturation of poly(rU) annealed to itself; this phenomenon has been reported (17). This is evidence against DNG binding to RNA in a nonspecific manner. Therefore, DNG maintains base-pair specificity while dramatically increasing its affinity for RNA compared with DNA·RNA complexes.

Our thermal denaturation results were reduced to the unit term of t_m per base pair in order to be able to compare t_m values for DNG bound to RNA with results of others for DNA bound to modified oligonucleotides. The plot of t_m per base pair vs. ionic strength (Fig. 2) exemplifies the differences between the thermal stability of DNG·RNA and the analogous DNA·RNA complexes. Not only does thymidyl DNG have a tremendously higher affinity than thymidyl DNA for poly(rA) over a wide range of ionic strengths, but the effect of ionic strength is much more pronounced for the DNG results. Most noteworthy is the observation that the effect of ionic strength on stability is the opposite for DNG·RNA as compared to DNA·RNA. Thus, while DNA·RNA duplexes become more stable with increasing ionic strength, DNG·RNA triplexes and duplexes generally become more stable with decreasing ionic strength. This is

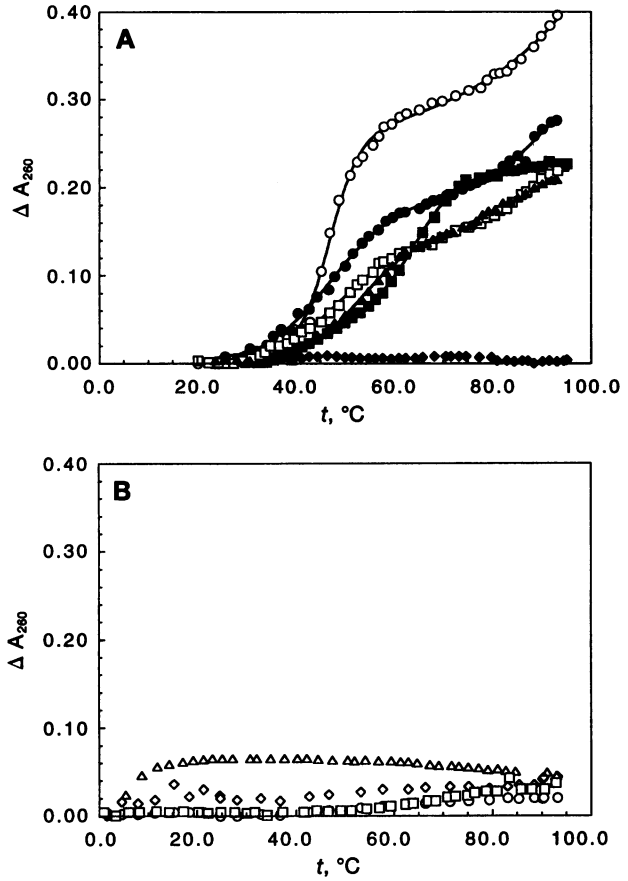

FIG. 1. (*A*) Plots of ΔA_{260} vs. t for d(Tg)$_4$T-azido (**1**) in the presence of poly(rA) at pH 7.0 (0.01 M $KHPO_4$ buffer). The ionic strength was held constant at 0.12 (◆), 0.22 (■), 0.42 (○), 0.62 (●), 0.82 (□), and 1.20 (▲) with KCl. (*B*) Plots of ΔA_{260} vs. t for d(Tg)$_4$T-azido (**1**) in the presence of poly(rG) (○), poly(rI) (□), poly(rC) (◇), or poly(rU) (△) at pH 7.0 (0.01 M $KHPO_4$ buffer) and μ = 1.2. The concentration of each oligonucleotide was 41.7 μM in bases. Data points were collected in ≈1°C increments at ≈5-min intervals. The curves through the data points in *A* were computer generated from either Eq. **1**, which optimizes for a single inflection point (t_{m1}), or Eq. **2**, which optimizes for two inflection points (t_{m1} and t_{m2}).

expected since increased salt concentration will effectively mask the opposing rows of negative charges on DNA·RNA hybrids, allowing a more stable duplex. Decreased salt concentration allows the oppositely charged backbones of the DNG·RNA hybrid to become intimately salt paired, thus stabilizing the complex. This effect has been alluded to with a positively charged oligonucleotide derivative binding to DNA (18).

Equilibrium Complexes of Thymidyl DNG with Poly(adenyl) Nucleic Acids. To complement the stoichiometry of **1** binding to poly(rA) and poly(dA) as determined from the thermal denaturation studies, the method of continuous variation (12) was used to generate mixing curves of the absorbance vs. mole percent of d(Tg) (single guanidinium-linked 2′-deoxyribothymidyl unit). This method is based on the assumption that the decrease in absorbance is proportional to the number of base pairs hydrogen bonded between the interacting species. Mixtures of **1** with poly(rA) at μ = 0.12 and 30°C (Fig. 3) reach a minimum absorbance at a mole fraction of ≈0.67 d(Tg) to 0.33 r(Ap) (single phosphate-linked riboadenyl unit). These results indicate that triple-stranded complexes were formed that contained two d(Tg) per r(Ap). The fact that the minima occur at the intersection of two straight lines through the data points is indicative of a reversiblyformed structure consisting of no unoccupied sites (19). At 60 and

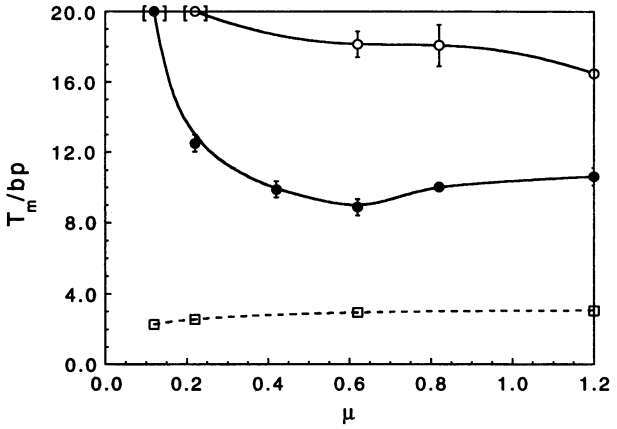

FIG. 2. Plot of t_m per base pair vs. μ at pH 7.0 (0.01 M $KHPO_4$ buffer) for denaturation of d(Tg)$_4$T-azido (● and ○ for the first and second transitions, respectively) and d(Tp)$_{15}$T (□) complexed to poly(rA). The ionic strengths were held constant by using 0.11, 0.21, 0.41, 0.61, 0.81, and 1.19 M KCl. The data points at the lowest ionic strength for DNG (enclosed in brackets) were simply taken as 100°C because no hyperchromic transition was apparent by 93°C.

90°C, the data points for the mixing curves of d(Tg) with r(Ap) again form two lines that intersect sharply at ≈67% (data not shown). This confirms the stable triple-helical nature of the DNG·RNA complexes at μ = 0.12 suggested by the lack of hyperchromic shifts in the thermal denaturation studies from 30 to 90°C.

The mixing curve for d(Tg) with d(Ap) (single phosphate-linked 2′-deoxyriboadenyl unit) at 30°C and μ = 0.12 is also centered near a mole fraction of ≈0.67 d(Tg) to 0.33 d(Ap) (Fig. 3). Unlike the experiments with r(Ap), this mixing curve has a rounded minimum, indicating that the dissociation reaction is too slow to allow overlapping sequences to adjust such that the maximum number of sites could be occupied (19). The smaller change in absorbance seen when d(Tg) interacts with d(Ap) compared to r(Ap) (Fig. 3) is also indicative of some binding sites remaining unoccupied. Equilibrium complexes are the same from 30 to 90°C since the mixing curves at 60 and 90°C (data not shown) for d(Tg) mixing with d(Ap) are similar to the 30°C results.

Molecular Models of Thymidyl DNG Complexes with RNA Strands. The ABNR minimization algorithm in the molecular mechanics program CHARMM was used with constraints to

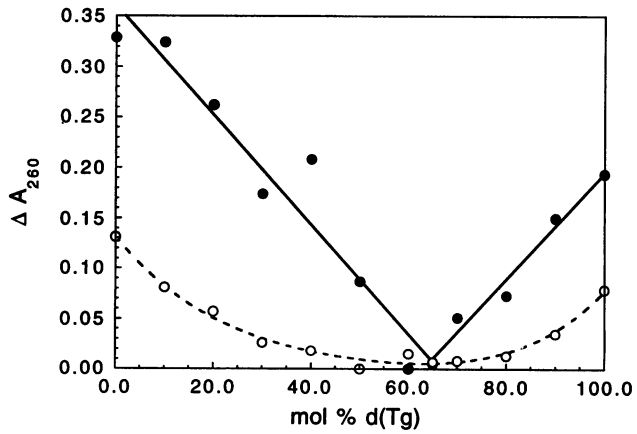

FIG. 3. Plots of ΔA_{260} vs. mol % d(Tg) (mixing curves) for d(Tg)$_4$T-azido with poly(rA) (●) and poly(dA) (○) at 30°C, pH 7.0, μ = 0.12. The inflection points indicate the stoichiometry of the complexes.

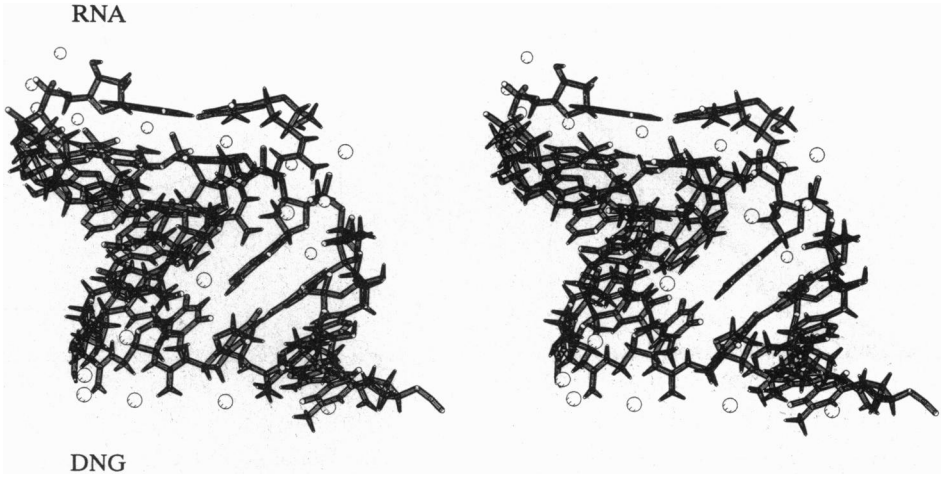

FIG. 4. Stereoview of the duplex hybrid r(Ap)$_9$A·d(Tg)$_9$T-azido. The model was computer generated from the structure of A-form d(Ap)$_9$A·d(Tg)$_9$T by changing the H2′ groups of the purine strand into hydroxyl groups, replacing the phosphate linkages with guanidinium groups, and using the ABNR algorithm to minimize using CHARMM.

yield models of one or two DNG molecules annealed to a single molecule of RNA. Counterions used remained proximal to their respective charged groups [Cl^- to guanidinium's -NH^+ were within 2.3 Å, whereas Na^+ were less than 2.9 Å from phosphate's —(PO_2^-)—]. Base pairing was considered maintained since the hydrogen bonds between the base pairs are all within 2.0 Å from donor to acceptor atom for Watson–Crick interactions and <2.2 Å for Hoogsteen interactions.

The results of thermal denaturation studies (*vide supra*) suggest that DNG oligomers can form two types of hybrids with complementary RNA strands. At high temperatures, one equivalent of DNG is annealed to one RNA equivalent (Fig. 1) via a Watson–Crick base pairing scheme (thymine O4 to adenine H7 and thymine H3 to adenine N1). A model for r(Ap)$_9$A·d(Tg)$_9$T-azido (Fig. 4) is based on the structure of complementary strands of RNA. An A-type polynucleotide structure is generally maintained with all sugars of both strands in the C3′ endo conformation except for the DNG terminal sugar, which is attached to the azido functionality; this sugar is in the O4′ endo conformation. In addition, this short and wide structure has an axial rise of only 2.4 Å per nucleotide, which also suggests an A conformation (20). A comparison of groove widths for the DNG·RNA duplex relative to the RNA·RNA analog shows that the major groove width increases by nearly 2.5 Å while the minor groove contracts by 1.4 Å. This is due to the electrostatic attractions rather than repulsions found in the different nucleic acid backbones.

At low temperatures, two equivalents of DNG anneal to a single equivalent of RNA (Fig. 1). The first strand of DNG is Watson–Crick base paired to RNA much as for the DNG·RNA duplex while the second strand is annealed via Hoogsteen base pairs (thymine O4 to adenine H6 and thymine H3 to adenine

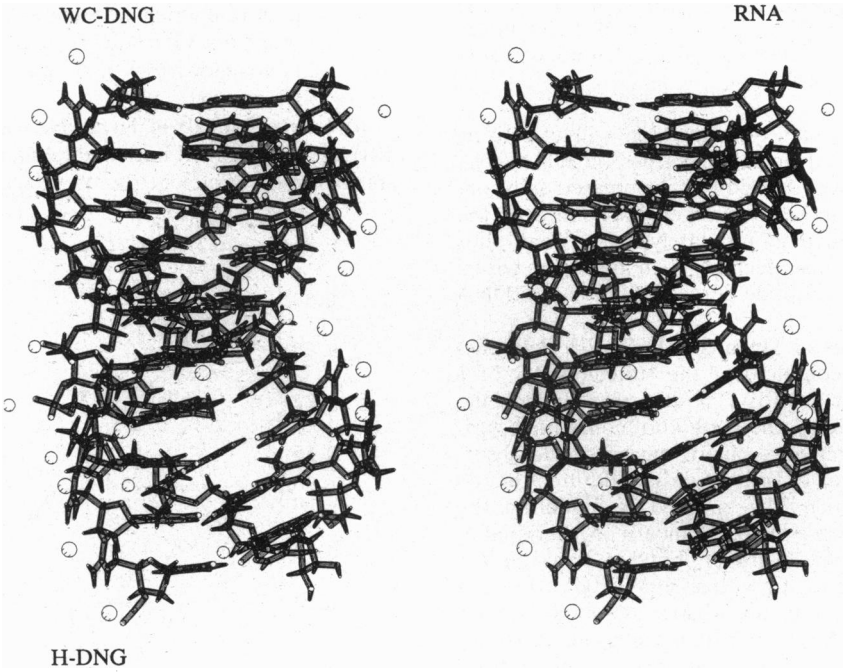

FIG. 5. Stereoview of the triple-helical structure of d(Tg)$_9$T-azido·r(Ap)$_9$A·d(Tg)$_9$T-azido. The minor groove can be seen near the top left of the figure, bordered by the RNA and Watson–Crick-paired DNG (WC-DNG) strands. The major groove is filled by the Hoogsteen-paired DNG (H-DNG) strand as can be seen near the bottom of the figure. The model was computer generated starting with the coordinates of Raghunathan *et al.* (13) for d(pT)$_{10}$·d(pA)$_{10}$·d(pT)$_{10}$. Modeling was carried out as described in Fig. 4 and in *Materials and Methods.*

N7). The model for the triple-helical decamer d(Tg)$_9$T-azido·r(Ap)$_9$A·d(Tg)$_9$T-azido presented in Fig. 5 is based on the model of d(pT)$_{10}$·d(pA)$_{10}$·d(gT)$_{10}$ (8). The sugars of the RNA strand are predominately puckered in the C2′ endo or C2′ endo/C4′ endo twist conformations while both strands of DNG are in the C2′ endo conformation, except at the azido termini where the sugars are again C4′ endo. This is suggestive of a B-type polynucleotide structure as is the relatively long (3.2 Å per nucleotide) axial rise (20). The structure of d(Tg)$_9$T-azido·r(Ap)$_9$A·d(Tg)$_9$T-azido is compact relative to both d(pT)$_{10}$·d(pA)$_{10}$·d(gT)$_{10}$ (8) and d(pT)$_{10}$·d(pA)$_{10}$·d(pT)$_{10}$ (13). The major and minor grooves of d(Tg)$_9$T-azido·r(Ap)$_9$ A·d(Tg)$_9$T-azido are 2.1 and 0.3 Å narrower than those of d(pT)$_{10}$·d(pA)$_{10}$·d(pT)$_{10}$ and 0.3 and 1.4 Å narrower than those of d(pT)$_{10}$·d(pA)$_{10}$·d(gT)$_{10}$.

From the above discussion, the following conclusions can be drawn about DNG: (*i*) thymidyl DNG is specific for its complementary tracts of adenine bases and does not interact with guanylic, cytidylic, or uridylic tracts; (*ii*) due to electrostatic attractions in the place of electrostatic repulsions, DNG binds to RNA with a much greater affinity than DNA to RNA; (*iii*) the thermal stability of DNG·RNA hybrid structures is attenuated by increasing salt concentrations; (*iv*) DNG appears suited for use as either an antigene (9, 10) or an antisense agent since it always forms a triple-helical structure under near-physiologic conditions (37°C, pH 7.0, and $\mu = 0.22$); (*v*) while a triple helix consisting of two d(Tg) to one r(Ap) has a similar stability to the corresponding DNG$_2$·DNA complex, a DNG duplex with RNA is more stable than the corresponding DNG·DNA complex; and (*vi*) molecular modeling suggests that the DNG strands take on the general conformation of the nucleic acid backbone to which they bind and that the overall structure of the hybrid complexes is more compact than that found in the homopolymeric RNA complexes.

This study was supported by grants from the National Institutes of Health and the Office of Naval Research.

1. Uhlmann, E. & Peyman, A. (1990) *Chem. Rev.* **90,** 543–584.
2. Crooke, S. T. (1992) *Annu. Rev. Pharmacol. Toxicol.* **32,** 329–376.
3. Crooke, S. T. (1993) *FASEB J.* **7,** 533–539.
4. Cook, P. D. (1993) in *Antisense Research and Applications*, eds. Crooke, S. T. & Lebleu, B. (CRC, Boca Raton, FL), pp. 149–187.
5. Sanghvi, Y. S. & Cook, P. D. (1993) in *Nucleosides and Nucleotides as Antitumor and Antiviral Agents*, eds. Chu, C. K. & Baker, D. C. (Plenum, New York), pp. 311–324.
6. Nielsen, P. E., Egholm, M., Berg, R. H. & Buchardt, O. (1991) *Science* **254,** 1497–1500.
7. Almarsson, Ö., Bruice, T. C., Kerr, J. & Zuckermann, R. N. (1993) *Proc. Natl. Acad. Sci. USA* **90,** 7518–7522.
8. Dempcy, R. O., Almarsson, Ö. & Bruice, T. C. (1994) *Proc. Natl. Acad. Sci. USA* **91,** 7864–7868.
9. Dempcy, R. O., Browne, K. A. & Bruice, T. C. (1995) *J. Am. Chem. Soc.* **117,** 6140–6141.
10. Dempcy, R. O., Browne, K. A. & Bruice, T. C. (1995) *Proc. Natl. Acad. Sci. USA* **92,** 6097–6101.
11. Riley, M., Maling, B. & Chamberlin, M. J. (1966) *J. Mol. Biol.* **20,** 359–389.
12. Job, P. (1928) *Ann. Chim.* **9,** 113–203.
13. Raghunathan, G., Miles, H. T. & Sasisekharan, V. (1993) *Biochemistry* **32,** 455–462.
14. Luger, P. & Paulsen, H. (1976) *Acta Crystallogr. B* **32,** 2774–2779.
15. Allen, F. H., Kennard, O. & Taylor, R. (1983) *Acc. Chem. Res.* **16,** 146–153.
16. Prive, G. G., Yanagi, K. & Dickerson, R. E. (1991) *J. Mol. Biol.* **217,** 177–199.
17. Young, P. R. & Kallenbach, N. R. (1978) *J. Mol. Biol.* **126,** 467–479.
18. Letsinger, R. L., Singman, C. N., Histand, G. & Salunkhe, M. (1988) *J. Am. Chem. Soc.* **110,** 4470–4471.
19. Felsenfeld, G. (1958) *Biochim. Biophys. Acta* **29,** 133–144.
20. Saenger, W. (1984) in *Principles of Nucleic Acid Structure*, ed. Cantor, C. R. (Springer, New York), p. 238.